Am J Physiol Cell Physiol 323: C14–C28, 2022.
First published May 25, 2022; doi:10.1152/ajpcell.00394.2021

american physiological society

AMERICAN JOURNAL OF PHYSIOLOGY
CELL PHYSIOLOGY

RESEARCH ARTICLE

An increase in force after stretch of diaphragm fibers and myofibrils is accompanied by an increase in sarcomere length nonuniformities and Ca^{2+} sensitivity

Massimo Contini,[1] David Altman,[2] Anabelle Cornachione,[3] Dilson Etcheverry Rassier,[4] and Maria Angela Bagni[1]

[1]*Department of Experimental and Clinical Medicine, University of Florence, Florence, Italy;* [2]*Department of Physics, Willamette University, Salem, Oregon;* [3]*Department of Physiological Sciences, Federal University of São Carlos, São Paulo, Brazil; and* [4]*Department of Kinesiology and Physical Education, McGill University, Montreal, Quebec, Canada*

Abstract

When muscle fibers from limb muscles are stretched while activated, the force increases to a steady-state level that is higher than that produced during isometric contractions at a corresponding sarcomere length, a phenomenon known as residual force enhancement (RFE). The mechanisms responsible for the RFE are an increased stiffness of titin molecules that may lead to an increased Ca^{2+} sensitivity of the contractile apparatus, and the development of sarcomere length nonuniformities. RFE is not observed in cardiac myofibrils, which makes this phenomenon specific to certain preparations. The aim of this study was to investigate whether the RFE is present in the diaphragm, and its potential association with an increased Ca^{2+} sensitivity and the development of sarcomere length nonuniformities. We used two preparations: single intact fibers and myofibrils isolated from the diaphragm of mice. We investigated RFE in a variety of lengths across the force-length relationship. RFE was observed in both preparations at all lengths investigated and was larger with increasing magnitudes of stretch. RFE was accompanied by an increased Ca^{2+} sensitivity as shown by a change in the force-pCa^{2+} curve, and increased sarcomere length nonuniformities. Therefore, RFE is a phenomenon commonly observed in skeletal muscles, with mechanisms that are similar across preparations.

cross-bridge model; diaphragm; myofibrils; sarcomeres; single fibers

INTRODUCTION

When a muscle fiber is stretched while activated, the force increases and stabilizes at a level that is higher than that produced during isometric contractions developed at a corresponding sarcomere length. This residual force enhancement (RFE) is present in skeletal muscle fibers (1–3), myofibrils (4–6), sarcomeres (7), and half-sarcomeres(8), with increases in force of up to ~28%–30%. However, RFE is not observed in cardiac muscles; well-controlled studies with isolated myofibrils from either ventricle (4) or papillary muscles (6) have failed to find an enhancement in force after stretch, a result that was confirmed in a study using the whole, intact cardiac trabeculae (9). This difference has been interpreted in light of a mechanism of the RFE, an increase in the stiffness of titin induced by activation and stretch—referred to as static tension (4, 6, 9). Although the static tension is present in skeletal muscles, it is not observed in cardiac muscles (4), likely due to different physiological demands. It is now clear that the RFE is caused by a combination of the static stiffness and sarcomere length nonuniformities that happen during activation and stretch (5, 7, 10), such that some sarcomeres will have a larger than anticipated overlap and active force production, whereas others will increase their passive force significantly (11). In addition, the static stiffness—nonrelated to cross bridges—has been associated with an increase in the stiffness of the elastic protein titin, which increases with the presence of Ca^{2+} (12) and during activation of skeletal muscles, but not cardiac muscles (4, 13).

When comparing striated muscles, there is still a gap in the literature; there are no studies looking into the presence and potential mechanisms of RFE in the diaphragm muscle. The diaphragm has characteristics that are unique: it is a respiratory muscle that contracts rhythmically against elastic and resistive forces, such that in each relaxation the diaphragm returns to a relatively constant length at a resting position, determined by the balance of lung and chest wall recoil forces (14). Limb muscles also contract rhythmically during locomotion, but they must overcome predominantly inertial forces. The most prominent feature of the diaphragm is the fact that, like the heart, it must contract in a repetitive rhythm during a lifetime. Although the differences between elastic, resistive, and inertial forces cannot likely explain differences in

Correspondence: M. A. Bagni (mangela.bagni@unifi.it); D. E. Rassier (dilson.rassier@mcgill.ca).
Submitted 1 November 2021 / Revised 17 May 2022 / Accepted 17 May 2022

RFE, they still provide the diaphragm with unique contractile characteristics.

In this study, we evaluated the potential presence and mechanism of RFE in the diaphragm. We took advantage of two unique preparations from our laboratories that allow the evaluation of the cellular and subcellular mechanisms of RFE: intact living fibers and isolated myofibrils from the mice. Intact fibers permit the evaluation of muscle mechanisms using the smallest contractile system that still maintains its main physiological characteristics (15–19); the fibers can be activated by electrical stimulation, which initiates action potentials, and can be experimented for many contractions. Myofibrils allow the control of the media surrounding the preparations while rapidly activating and relaxing the contractile system, the direct measurement of individual sarcomere lengths, and a precise measurement of specific force given its small cross-sectional area (~1 μm) (5, 6, 20, 21). We observed RFE in the diaphragm, which was accompanied by an increase of sarcomere length nonuniformities and myofibrillar Ca^{2+} sensitivity of the contractile apparatus. The result lead us to develop a stochastic model to understand how sarcomere length nonuniformities and an increase in the stiffness of titin in a myofibril can lead to RFE. Using this model, we were able to reproduce our experimental observations.

METHODS

In this study, we used small bundles with intact diaphragm fibers and isolated diaphragm myofibrils from the mouse. The animal protocol for the work with mice intact fibers was undertaken in compliance with the guidelines of the European Communities Council Directive 2010/63/UE and the recommendations for the care and use of laboratory animals and it was approved by the animal care Committee of the University of Florence (Italy) and Italian health Ministry (Authorization 708/2017-PR). The animal protocol for the mice myofibrils was approved by the Animal Care Committee at McGill University and the Canadian Council on Animal Care (Reference No.: 20122-23).

Intact Fiber Preparation

Experiments with intact fibers were performed using CD1 mice (Envigo, RMS Srl, Udine, Italy). Animals were housed with a controlled temperature (21°C–24°C) and a 12-12 h light-dark cycle. Food and water were provided ad libitum. Female mice (7–8 mo old) were killed by prompt cervical dislocation to minimize animal suffering. The diaphragm muscle was quickly excised and placed in Tyrode solution with the following composition (mM): NaCl, 121; KCl, 5; CaCl2, 1.8; MgCl2, 0.5; NaH2PO4, 0.4; NaHCO3, 24; glucose, 5.5; and EDTA, 0.1 and bubbled with 5% CO_2–95% O_2 which gave a pH of 7.4. Small bundles were dissected from the diaphragm, as described previously (15, 22, 23). The dissection was performed manually under a stereomicroscope with a fine pair of scissors taking care to avoid stretching and to obtain preparations clean of debris from dead fibers. Small aluminum T-shaped clips were fixed to the tendons as close as possible to the fiber ends. The fibers were transferred to a temperature-controlled experimental chamber (801 C/1900, Aurora Scientific, Toronto, Canada) and mounted on an inverted microscope (Olympus IX71). The clips attached the fibers horizontally between the lever arms of a capacitance force transducer (405 A, Aurora Scientific) and a length controller (322 Aurora Scientific). The fibers were superfused continuously with oxygenated Tyrode solution by a peristaltic pump. The experiments were performed at 27°C–28°C.

The resting bundle length, the bundle's largest and smallest diameters were measured with a microscope fitted with ×20 eyepieces and a ×5 dry objective in the experimental chamber. The preparation length in our fibers (L_o, clip to clip) was 9.6 ± 0.68 mm (means ± SE, n = 15), of which 8.6 ± 0.66 mm was composed of the fibers and the remaining (0.99 ± 0.22 mm) was composed of tendons. The cross-sectional area of the bundles was calculated as a × b × π/4, where a and b are the average values of the width and the vertical height of the preparations, respectively, measured at 2–3 different points along the bundles. The average cross-sectional area of the fiber bundles was 0.08 ± 0.01 mm^2.

Experimental protocol.

After a 15-min equilibration period, bipolar stimuli (1-ms duration at 1.5 times threshold voltage) were applied across the fibers by two platinum-plate electrodes mounted parallel to the bundle via a high-power bipolar stimulator (701 C Aurora Scientific). After testing the fibers viability, in which tetanic stimulation (1-s duration) was applied at 1-min intervals using the minimum frequency necessary to obtain a fused contraction (100 Hz), the fibers were set at a length (L_o) at which tetanic force was maximal (P_o). In the current experiments, this length corresponded to a mean sarcomere length of ~2.70 μm. Tetani were given for a period of ~10 min; if P_o decreased by >15%, the fibers were discarded. Following the stabilization period, one of the two protocols was used:

1) Bundles were subjected to two different series of contractions (3.5 s in duration, elicited every 2 min). During the first protocol, starting from L_o, the bundles were stretched first to reach a new length the L_i length at which the tetanic tension produced was just lower than P_o, and then passively stretched by 4% and 8% of L_o to reach the final length L_f. At this length, L_f, a tetanic contraction was elicited. The entire sequence of stretches and contractions was repeated but only after a new L_i length was reached. Every time the new starting L_i length was a little bit longer and the corresponding developed tension was a little bit lower than the previous one. It was estimated that we would have a 6% decrement of tension between each pair of L_i value. In this way for each bundle and for the different stretch amplitudes tested, it was possible to obtain more than one point of measure, exploring the descending limb in terms of RFE as far as the saturation transducer permitted. Between contractions produced at different L_i, tetanic reference contractions were performed to check whether the isometric maximal P_0 force produced at L_o was constant throughout the experiments.
2) A second series of contractions were performed to evaluate the RFE. The duration of these contractions was sufficient to reach steady-state forces the following stretch, i.e., when the force-time trace following active stretch was parallel to the force-time trace of the corresponding isometric contraction. In this series of contractions,

starting from L_i, the bundle was stimulated and an active variable stretch, $L_i + \%$, was applied at the tetanic plateau.

The RFE was measured as the difference between the two traces $L_i + \%$ and L_f, 100 ms before the end of stimulation. Figure 1 shows an example from an experiment conducted to evaluate the RFE, with an isometric contraction and a contraction in which a stretch (4% L_o) was applied to the fiber. Passive and active stretches were applied in amplitudes of 4% and 8% of L_o (stretch durations of 0.2 s and 0.4 s, respectively).

In summary, one full stretch experiment consisted of the following tests: isometric contractions at L_0, L_i, and L_f; passive and active stretches starting from L_i. Following, a next stretch experiment at a new L_i was performed. The whole experimental protocol induced a large number of contractions, but it is known that the maximal force developed by intact muscle bundles remains stable for many hours when the fibers are stimulated at regular intervals (2 min) with tetanic stimulation frequency (100 Hz) (22, 24).

The output of the force transducer and the length controller were acquired in real time using an integrated PC board (NI6221, National Instruments). The experimental data were displayed and successively analyzed with a dedicated controlled software (600 A Digital controller, Aurora Scientific, Canada).

Since *1*) changes in fiber length in muscle bundles do not correspond exactly to changes in sarcomere length across experiments, and may lead to comparisons of contractions made at very different lengths, and *2*) there is a large variability in the force-length relationship obtained with contractions developed using fixed-end experiments (i.e., when sarcomere length is not controlled during the experiments), an estimation of length variations in the diaphragm bundles was derived from the L_i/P_0 ratio—the force produced at L_i relative to the force developed at L_o. In this way, we guaranteed that we were comparing contractions produced when the isometric forces were similar if compared with the forces produced at the respective L_o, and therefore produced at comparable fiber lengths. All the RFE measures obtained during the experiments were grouped into five classes with intervals of 10% L_i/P_0. Before grouping, each value was expressed in terms of specific force mN/mm^2. Then the average value of each class was plotted.

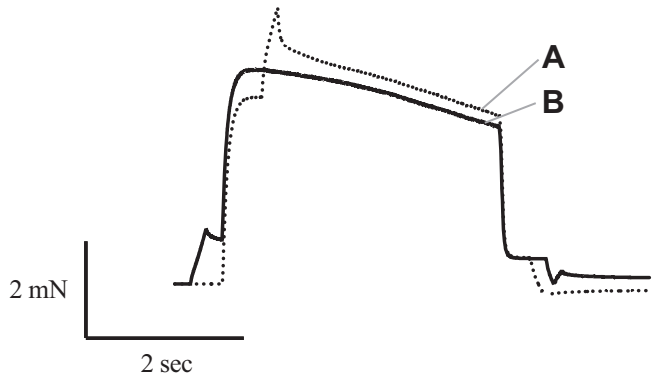

Figure 1. Typical contractions produced by a bundle of intact fibers, developed at L_f and at $L_i + 4\%$, starting from the same L_i. The solid line indicates the isometric contraction Lf, and the dotted line indicates the contraction with an active stretch imposed during activation Li + 4%. Stretch amplitude was 4%. A and B indicate the points where the forces were measured, at 100 ms before the end of stimulation.

Myofibril Preparations

Experiments with myofibrils were performed with CD1 mice (Charles River, Canada). Small muscle bundles of the diaphragm muscle were dissected, tied to wood sticks, and chemically permeabilized following standard procedures used in our laboratory (6, 21, 25, 26). Muscles were incubated in rigor solution (pH = 7.0) for ~4 h, after which they were transferred to a rigor: glycerol (50:50) solution for ~15 h. The samples were subsequently placed in a fresh rigor: glycerol (50:50) solution with the addition of a cocktail of protease inhibitors (Roche Diagnostics) and stored in a freezer (−20°C) for at least 7 days. On the day of the experiments, small pieces of the samples were homogenized following standard procedures, which resulted in a solution containing isolated myofibrils. The myofibrils were transferred to the experimental setup, which contained a system for the detection of atomic force cantilever (AFC) displacements (27).

Measurements of myofibril forces.

The myofibrils were attached between the AFC and a rigid glass needle. A multichannel fluidic system connected to a double-barreled pipette was used for fast activation and relaxation of the myofibrils. During the experiments, the position of the double-barreled pipette was rapidly switched to change the solutions surrounding the myofibrils (pCa 4.5 and pCa 9.0; $pCa = -\log_{10}[Ca^{2+}]$). Such a procedure allows for a fast activation and relaxation of the myofibrils without damages to the preparation, and has been explained in detail in previous studies (6, 21, 25, 26). Under high magnification, the contrast between the dark bands of myosin (A-bands) and the light bands of actin (I-bands) provided a dark-light intensity pattern, representing the striation pattern produced by the sarcomeres, which allowed measurements of sarcomere length during the experiments. The sarcomere length was measured with a video camera connected to the right-side port of the microscope. Once the myofibrils were attached between the AFC and the microneedle, they were adjusted to an average sarcomere length of 2.7 μm. Throughout the experiments, homogeneity of sarcomere length was assessed visually to detect potential damage in the myofibrils. When nonuniformity of sarcomere lengths formed during activation did not recover into a regular striation pattern before the next activation, the experiment was stopped and the myofibril was discarded from further analysis.

The myofibril length was more variable than the intact fiber length during the experiments, as myofibrils of distinct lengths were produced during the homogenization protocol and were selected based on their appearance; the length was 19.16 ± 5.31 μm (means ± SE, total n in all protocols used in this study = 23). The cross-sectional area of the myofibrils, calculated using a method similar to that used in intact fibers, was 1.07 ± 0.14 μm.

Solutions. The rigor solution (pH 7.0) used to store the myofibrils was composed of (in mM): 50 Tris, 100 NaCl, 2 KCl, 2 $MgCl_2$, and 10 EGTA. The relaxing solution used for

muscle dissection (pH 7.0) was composed of (in mM) 100 KCl, 2 EGTA, 20 imidazole, 4 ATP, and 7 $MgCl_2$. The experimental solutions used during the experiments (pH 7.0) were composed of (in mM) 20 imidazole, 14.5 creatine phosphate, 7 EGTA, 4 MgATP, 1 free Mg^{2+}, free Ca^{2+} ranging from 1 nM (pCa 9.0) to 32 μM (pCa 4.5), and KCl to adjust the ionic strength to 180 mM. The final concentrations of each metal-ligand complex were calculated using a computer program used in previous studies (13, 26, 29). All experiments were performed at 25°C–27°C.

Force and sarcomere length calculations.

Force measurement using the AFC was performed as previously described (26, 27). Briefly, a laser is shined upon and reflected from the AFC, which acts as a force transducer. When an attached myofibril is shortened due to activation, it causes deflections of the AFC, which are detected and recorded using an optical system with a time resolution in the order of milliseconds. The force produced by a single sarcomere is equivalent to that of a single myofibril and was calculated using:

$$F(t) = k_C * c(t), \quad (1)$$

where $F(t)$ is the force per myofibril as a function of time (t), $c(t)$ is the displacement of the cantilever tip (sampling rate: 0.2 MHz averaged over 1,280 data points), and k_C is the stiffness of the silicon cantilever. The cantilever stiffness was determined either by measuring the cantilever dimensions through scanning electron microscope images, or by constructing force-bending curves using cantilevers previously calibrated with the scanning electron microscope images (6, 21). The sarcomere length of the myofibrils was calculated using:

$$S(t) = \left(M(0) - \left[c(t) - c(0)\right] + \left[n(t) - n(0)\right]\right)/S_N, \quad (2)$$

where $S(t)$ represents the average sarcomere length as a function of time and captures the central tendency of the sarcomeres given any nonuniformity in the sarcomere length behavior. Moreover, $M(0)$ is the myofibril length at rest, $c(0)$ is the initial position of the cantilever tip, $n(t)$ is the input motion of the micro-needle, $n(0)$ is the initial position of the microneedle, and S_N is the number of sarcomeres within the myofibril.

The random errors in $F(t)$ and $S(t)$ were minimized in four ways. First, cantilever displacement was calibrated before the start of each experimental set using the laser-tracking system. Second, the microneedle was at least 20 times thicker than the cantilever and did not deflect during the experiments. Third, the microneedle was controlled by a piezoelectric controller with a resolution greater than the noise of the system and did not limit the detectability of the myofibril response. Fourth, myofibrils with a large number of sarcomeres were studied so that the SL could better represent the central tendencies of the sarcomeres, despite any nonuniformity in behavior.

Experimental protocol.

RFE was measured using a protocol that was similar to that one used with intact fibers, with a few characteristic differences since we used the sarcomere length (instead of length changes as a percentage of L_o) to set the preparations through the experiments. The myofibrils (n = 12) were adjusted so that the nominal average sarcomere length was 2.7 μm (actual: 2.74 ± 0.15 μm, as verified after data analysis) before a contraction was induced by activation solution. After the onset of activation, contractions were held steady for 15 s before the surrounding solution was switched to the relaxing solution, which induced full relaxation.

After two control contractions (3-min interval), the myofibrils were set sarcomere lengths of 2.9 μm, and 3.0 μm in random order, and isometric contractions were induced at these lengths. Finally, the myofibrils were set at lengths of 2.7 μm, 2.8 μm, or 2.9 μm, and stretched to 2.9 μm or 3.0 μm (stretch magnitudes of ~4% or 8%, respectively). Stretches were induced at a speed of 0.3 μm/s during force production to reach a sarcomere length similar to the isometric contraction at L_f. After stretch, an isometric contraction was repeated again to check for the potential damage to the myofibril.

Force-pCa^{2+} relationship and Ca^{2+} sensitivity of the contractile apparatus.

We performed additional experiments with myofibrils (n = 9) to check for the Ca^{2+} sensitivity of the contractile apparatus after stretch, and during the development of RFE. For these experiments, we first set the myofibrils at a sarcomere length of 2.9 μm and exposed them to different Ca^{2+} concentrations (pCa^{2+} of 7, 6.5, 6, 5.75, 5.5, 5, and 4.5). Then we performed experiments in which we stretched the myofibrils from 2.8 μm to 2.9 μm at the same Ca^{2+} concentrations. The two force-pCa^{2+} curves were fit to Hill's equation:

$$F = \left(Ca^{2+}/K\right)^{nH}/\left[1 + \left(Ca^{2+}/K\right)^{nH}\right] + F_{min} \times \left[1 - \left(Ca^{2+}/K\right)^{nH}/\left[1 + \left(Ca^{2+}/K\right)^{nH}\right]\right], \quad (3)$$

where F is the normalized force, K is the dissociation constant ($pK = -\log K$ = pCa50), nH is the Hill coefficient, and F_{min} is the minimum force levels at a high pCa^{2+}. pCa50 corresponds to the half-maximal force response, an index that we have used previously as an indicator of Ca^{2+} sensitivity (28).

Sarcomere length dispersion.

During the experiments with myofibrils, it was possible to measure the length of individual sarcomeres throughout the experimental procedures. Such measures allowed us to evaluate the sarcomere length dispersion and nonuniformity during activation and stretch in the different experimental conditions. The dispersion for each myofibril was found by calculating the difference of individual sarcomere lengths to the average sarcomere length of one myofibril, as follows:

$$SL_{dispersion} = |SL_{individual} - SL_{average}|. \quad (4)$$

Statistical Analysis

Forces produced by the fibers and myofibrils in similar lengths during isometric contractions and stretch contractions were compared using a two-way analysis of variance (ANOVA) for repeated measures. Sarcomere length dispersion between rest, activation, and after stretch was compared using a one-way ANOVA for repeated measures. The $pCa^{2+}{}_{50}$ obtained during isometric contractions or after stretch was compared using a one-way ANOVA for repeated measures. All post hoc analyses were performed with the Holm–Sidak test when needed (statistical package: SigmaPlot 13, Systat Software Inc., San Jose, CA). A significance value of 5% ($P < 0.05$) was adopted in all comparisons. Data are presented as means ± SE, or in box plots showing the also the interquartile ranges.

Stochastic Model of Residual Force Enhancement

Experimental results were reproduced in stochastic simulations of a myofibril.

These models were built up from the fundamental actomyosin interaction to the sarcomere levels, in which we were able to manipulate both sarcomere-nonuniformities and the changing stiffness of titin upon stretch. The model represents an extension of a previously described model (29), which is built upon the framework developed in a study by Campbell (30). We build up our model of a myofibril starting with the individual force-dependent actomyosin chemomechanical cycle. We then model a half-sarcomere as numerous myosin motors in parallel with one another and with a passive elastic element representing titin. Finally, we develop our model of a myofibril by connecting numerous half-sarcomeres in series. The values of all constants described in the model are presented in Table 1.

Model of an Individual Cross Bridge

The states in which the actomyosin system cycles are depicted in Fig. 2*A*, where *state 0* is a weakly associated state between the actin and myosin, and *states 1* and *2* are strongly associated stages, with the motor's power stroke occurring during the transition from *state 1* to *state 2*. The power stroke occurs over a distance d, and we define the distance from *state 1* to the transition state of the powerstroke transition to be δ_1 and the distance from *state 2* to this transition state to be δ_{-2}. We require $d = \delta_1 + \delta_{-2}$.

As indicated in Fig. 2*A*, all rates are modeled as force dependent except for the actin-attachment rates for the motor (k_0 and k_{-0}); the force-dependent rates are described in detail in the sections *Force-dependent rates associated with the power stroke* and *Force-dependent rates associated with the detachment of the motor from actin*. The cross bridge is modeled as a Hookean spring with stiffness κ_{cb}, and so the force that an individual motor experiences at a given extension of its cross bridge is given by:

$$F = -\kappa_{cb}\varepsilon, \tag{5}$$

where ε is the extension of the linear spring in the positive direction (which we have defined as the direction of the power stroke).

Force-dependent rates associated with the power stroke.

In the model, $k_1(F)$ is the rate associated with the power stroke. Assuming that the motor is experiencing a force in the negative direction due to a positive value of ε, the motor must do work against this opposing force to reach the transition state of the power stroke. Because the power stroke itself changes ε, this opposing force is not constant. However, we can calculate the average force that the motor experiences as it approaches the transition state to be:

$$F_{\text{forward}} = -\kappa_{cb}\left(\varepsilon + \frac{\delta_1}{2}\right) = F - \kappa_{cb}\frac{\delta_1}{2}, \tag{6}$$

where ε is the extension of the cross bridge before the power stroke. We then model this force-dependent rate using Bell's model (31),

$$k_1(F) = k_1(0)\exp\left(\frac{F_{\text{forward}}\delta_1}{k_BT}\right). \tag{7}$$

By a similar argument, we model the force dependence of the rate $k_{-2}(F)$, which describes the transition associated with reversing the power stroke. In this case, the average force that the motor experiences as it approaches the transition state in the reverse direction is:

$$F_{\text{reverse}} = -\kappa_{cb}\left(\varepsilon - \frac{\delta_{-2}}{2}\right) = F + \kappa_{cb}\frac{\delta_{-2}}{2}. \tag{8}$$

We again model this rate using Bell's model,

$$k_{-2}(F) = k_{-2}(0)\exp\left(-\frac{F_{\text{reverse}}\delta_{-2}}{k_BT}\right). \tag{9}$$

Force-dependent rates associated with the detachment of the motor from actin.

We model the force dependence of the rates associated with detachment from actin [$k_{-1}(F)$ and $k_2(F)$] assuming a catch-slip mechanism for actomyosin detachment, as described in a study by Guo and Guilford (32). According to this model, at low forces, the rate of detachment of the motor from actin decreases with force, whereas at larger forces, the rate increases. We describe this situation using two Bell-like terms, where the first term describes a rate that decreases with force and the second term describes a rate that increases with force:

$$k_2(F) = k_{2a}(0)\exp\left(-\frac{|F|\delta_{2a}}{k_BT}\right) + k_{2b}(0)\exp\left(\frac{|F|\delta_{2b}}{k_BT}\right) \tag{10}$$

$$k_{-1}(F) = k_{-1a}(0)\exp\left(-\frac{|F|\delta_{-1a}}{k_BT}\right) + k_{-1b}(0)\exp\left(\frac{|F|\delta_{-1b}}{k_BT}\right). \tag{11}$$

Model of a Half-Sarcomere

To determine the number of motors that can potentially interact with the thin filament in an activated half-sarcomere, we calculate the overlap of the thick and thin filaments as:

Table 1. *Constants associated with the chemomechanical cycle of a cross bridge and the mechanical properties of the cross bridge and the nonlinear passive spring element*

Parameter	Value
d	10 nm
k_0	12 s^{-1}
k_{-0}	0.05 s^{-1}
k_1 (0)	10 s^{-1}
δ_1	5 nm
k_{-1a}	40 s^{-1}
δ_{-1a}	0.75 nm
k_{-1b} (0)	0.25 s^{-1}
δ_{-1b}	0.375 nm
k_{2a} (0)	40 s^{-1}
δ_{2a}	2 nm
k_{2b} (0)	0.25 s^{-1}
δ_{2b}	3 nm
k_{-2} (0)	0.375 s^{-1}
δ_{-2}	5 nm
κ_{cb}	0.001 N/m
x_{offset}	900 nm
L	140 nm
σ	2,000 N/m^2

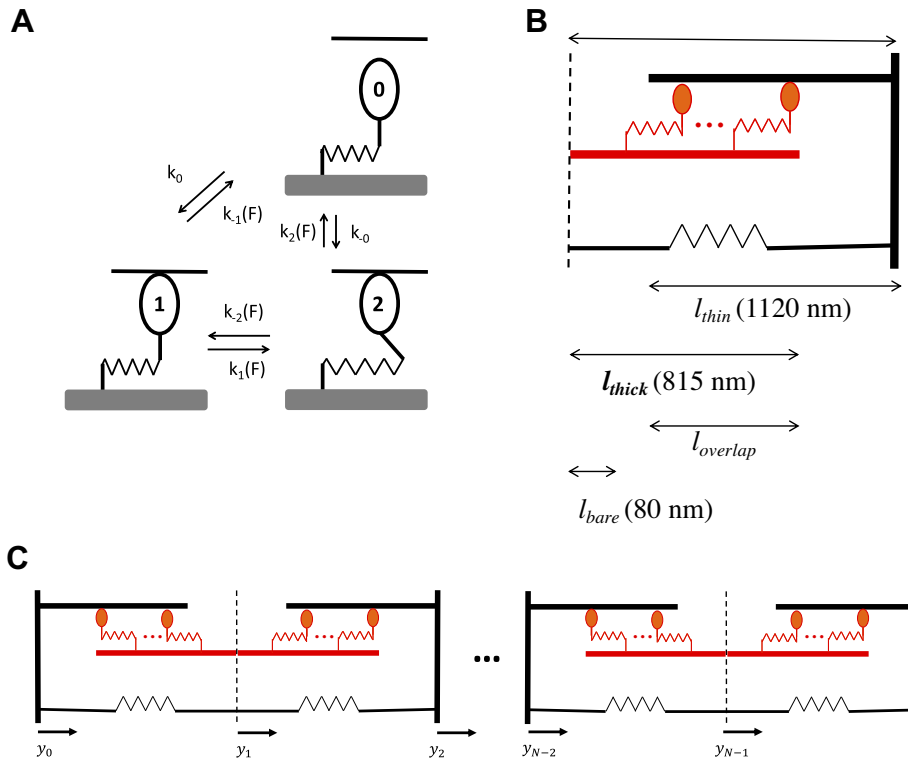

Figure 2. *A*: chemomechanical cycle for an individual cross bridge in an activated sarcomere. The transition from *state 1* to *state 2* is associated with the motor's power stroke. *B*: mechanical model for a single activated half-sarcomere, consisting of numerous cross bridges (represented by red springs) connected in parallel with one another. The cross bridges are also connected in parallel with a single passive element (titin; represented by a black spring). *C*: model of a myofibril has a series of *N* half-sarcomeres in series. The positions of the boundaries are represented by y_j, where $j = 0, 1, 2...N$.

$$x_{\text{overlap}} = l_{\text{thin}} + l_{\text{thick}} - x_{hs}, \quad (12)$$

where x_{hs} is the length of the half-sarcomere, and the other parameters describe the geometry of a half-sarcomere, as depicted in Fig. 2*B*.

The number of myosin heads per unit cross-sectional area in a single half-sarcomere framework is about $N_o = 1.15 \times 10^{17}$ m^{-2} (30, 33), and the cross-sectional area of the myofibril is about $A = 10^{-12}$ m^2. The number of motors that can engage with the thin filament are calculated as:

$$N_{\text{motors}} = AN_o\left(\frac{x_{\text{overlap}}}{x_{\text{max,overlap}}}\right) \quad x_{\text{overlap}} < x_{\text{max, overlap}}, \quad (13)$$

$$N_{\text{motors}} = AN_o \quad x_{\text{overlap}} > x_{\text{max, overlap}}$$

where

$$x_{\text{max,overlap}} = l_{\text{thick}} - l_{\text{bare}} = 735 \text{ nm}. \quad (14)$$

To investigate the effects of heterogeneities in half-sarcomere lengths on RFE, we needed to introduce variability in the half-sarcomere lengths. To this end, we used the approach taken in a study by Campbell (30), and assumed that the number of interacting myosin heads per half-sarcomere was a normally distributed variable with a variance that we could choose. To achieve this, we defined the actual number of interacting motors as:

$$N_{\text{interacting}} = G(\alpha)\ N_{\text{motors}}, \quad (15)$$

where $G(\alpha)$ is a number randomly selected from a normal distribution with a mean of one and a variance of α. The values of α used in our model are described in the section *Stochastic Simulations*.

We modeled each of the interacting motors as being connected in parallel with one another and with a passive nonlinear elastic element, representing titin. The force generated by stretching this nonlinear element is given by

$$F_{\text{nonlinear}}(x_{hs}) = \sigma A\ \exp\left(\frac{x_{hs} - x_{\text{offset}}}{L}\right). \quad (16)$$

Model of a Myofibril

Myofibrils consist of N half-sarcomeres connected in series. The $N + 1$ positions of each boundary are given by y_j, where $j = 0, 1, 2...N$ (Fig. 2*C*). The length of each half-sarcomere $x_{hs,\,i}$ is given by the relation:

$$x_{hs,i} = y_{i+1} - y_i, \quad (17)$$

where $i = 0, 1, 2...N - 1$.

Stochastic Simulations

Using the procedures described below, we compared three simulated conditions for myofibrils consisting of $N = 50$ half-sarcomeres:

1) Isometric activation of a myofibril at an average sarcomere length of 3 μm (average half-sarcomere length = 1.5 μm);
2) Isometric activation of a myofibril at an average sarcomere length of 2.8 μm (average half-sarcomere length = 1.4 μm) followed by a stretch of 0.1 μm/half-sarcomere at a rate of 0.1 μm/s/half-sarcomere; and
3) The same process as *2*), with the modification that, when the stretch is initiated, the stiffness of the nonlinear element increases. This adjustment is meant to capture the observation that, following activation, stretch of titin results in an increased stiffness in this nonlinear spring.

Isometric activation at half-sarcomere length of 1.5 μm.

Initial conditions. The boundaries of the N half-sarcomeres were set so that $y_0 = 0$ and $x_{hs,i} = 1.5$ μm for all values

of i. Because we assume that heterogeneities in half-sarcomere lengths arise as a result of stretch, throughout isometric activation, $\alpha = 0$. Before activation, all motors start in *state 0*. Upon activation, the motor is allowed to evolve into other states according to the rates described in Table 1 and *Eqs. 2–7*. The simulation proceeds iteratively through *Determine the number of interacting motors–Allow the myofibril to return to mechanical equilibrium*, using a time step of $\Delta t = 1$ ms.

Determine the number of interacting motors. We use the values of y_j to determine the length of each half-sarcomere $x_{hs,\,i}$ using *Eq. 17*. Then, using the process described in the section *Model of a Half-Sarcomere*, we calculate the number of interacting motors for each half-sarcomere. For a given half-sarcomere, if the number of interacting motors increases relative to the previous time step, additional motors, each in *state 0*, are incorporated into the model. If the number of interacting motors decreases relative to the previous time step, then the appropriate number of motors are removed.

Allow the state of each motor to evolve. Each interacting motor within a half-sarcomere starts in *state l*, where l = 0, 1, or 2. The probability of moving to the next state in the forward direction is given by

$$p_{\text{forward}} = k_l \Delta t, \tag{18}$$

and the probability of moving to the previous state in the backward direction is given by

$$p_{\text{backward}} = k_{-l} \Delta t. \tag{19}$$

The probability of remaining in the same state is thus given by

$$p_{\text{remain}} = 1 - p_{\text{backward}} - p_{\text{forward}}. \tag{20}$$

For each motor, a number n_{rand} is selected at random between 0 and 1, and a decision is made based on the following rules:

$$\begin{gathered}\text{The motor transitions from } \textit{state } l \text{ to } \textit{state } (l+1) \text{ if} \\ n_{\text{rand}} < p_{\text{forward}}. \\ \text{The motor transitions from } \textit{state } l \text{ to } \textit{state } (l-1) \text{ if} \\ p_{\text{forward}} < n_{\text{rand}} < p_{\text{forward}} + p_{\text{backward}} \\ \text{The motor remains in } \textit{state } l \text{ if} \\ n_{\text{rand}} > p_{\text{forward}} + p_{\text{backward}}\end{gathered} \tag{21}$$

Within half-sarcomere i, we also define a term $\varepsilon_{n,\,i}$, which describes the extension of the nth elastic cross-bridge linkage away from its equilibrium position. For a motor in *state 0*, $\varepsilon_{n,\,i}$ is set to 0. For a motor that transitions from *state 1* to *2*, $\varepsilon_{n,\,i}$ increases by d (indicating a power stroke). For a motor that transitions from *state* 2 to *1*, $\varepsilon_{n,\,i}$ decreases by d (indicating a reversal of the power stroke).

A motor that has just entered *states 1* or *2* from *state 0* is transitioning from a weakly actin-bound state to a strongly bound state. Due to thermal motion, the motor may not bind at zero extension. To account for this, we assign a value for $\varepsilon_{n,\,i}$ that is selected from a Gaussian distribution with mean zero and standard deviation of 7.5 nm.

Allow the myofibril to return to mechanical equilibrium. As a result of the motors' changing states, the system may be out of mechanical equilibrium. We allow the boundaries of the half-sarcomeres (y_j) to move to return to equilibrium. The only exception is that we do not allow y_0 or y_N (the ends of the myofibril) to move.

Specifically, before the boundaries are allowed to move, boundary y_j experiences a force in the negative direction from the half-sarcomere to its left. This force has magnitude:

$$F_{\text{left},j} = F_{\text{nonlinear}}(x_{hs,j-1}) + \sum_n \kappa_{cb}\varepsilon_{n,j-1}, \tag{22}$$

where the summation is over all the interacting cross bridges. It also experiences a force in the positive direction due to the half-sarcomere to its right, which has magnitude:

$$F_{\text{right},j} = F_{\text{nonlinear}}(x_{hs,j}) + \sum_n \kappa_{cb}\varepsilon_{n,j}. \tag{23}$$

As already discussed, as a result of the evolution of the motors in *Allow the state of each motor to evolve*, these two forces may not be in balance. We thus allow all the boundaries to move until mechanical equilibrium is restored, and $F_{\text{left},\,j}$ is equal to $F_{\text{right},\,j}$ for each boundary. To do this, we define the required displacement of the boundary y_j as Δy_j. The length of each half-sarcomere $x_{hs,\,i}$ changes as a result of these displacements according to the relation:

$$\Delta x_{hs,\,i} = \Delta y_{i+1} - \Delta y_i. \tag{24}$$

When the half-sarcomere changes its length, this also changes the extension of all attached motors (in *states 1* and *2*) by $\Delta x_{hs,\,i}$. For half-sarcomere i, we define the number of these attached motors as $N_{\text{attached},\,i}$.

As a result of these changes in the half-sarcomere lengths, the forces in *Eqs. 22* and *23* become:

$$\begin{aligned}F_{\text{left},j} = F_{\text{nonlinear}}\left(x_{hs,j-1} + \Delta x_{hs,j-1}\right) + \sum_n \kappa_{cb}\varepsilon_{n,j-1} \\ + N_{\text{attached},j-1}\kappa_{cb}\Delta x_{hs,j-1}\end{aligned} \tag{25}$$

$$\begin{aligned}F_{\text{right},j} = F_{\text{nonlinear}}\left(x_{hs,j} + \Delta x_{hs,j}\right) + \sum_n \kappa_{cb}\varepsilon_{n,j} \\ + N_{\text{attached},j}\kappa_{cb}\Delta x_{hs,j}.\end{aligned} \tag{26}$$

For each boundary, we require $F_{\text{left},\,j} - F_{\text{right},\,j} = 0$, which results in $N - 1$ equations which all must be satisfied at mechanical equilibrium (note that we do not have an equation for either the y_0 or y_N boundaries). We use a nonlinear solver in Python to find the values of Δy_j which satisfy these equations (34).

Once this process is complete, we modify our boundary positions using the resulting displacements, and we return to *Determine the number of interacting motors*. This process is repeated for 5 s.

Isometric activation of a myofibril at an average half-sarcomere of length 1.4 μm, followed by a stretch of 0.1 μm/half-sarcomere.

The initial conditions and the initial isometric activation occur identically as described in *Initial conditions*, except that $x_{hs,\,i} = 1.4$ μm. At 1 s, a stretch of the myofibril occurs at a rate of 0.1 μm/s/half-sarcomere until the half-sarcomeres reach an average length of 1.5 μm (after 1 s). To achieve this, during the stretch, each time-step starts with a displacement of the boundary at the end of the myofibril

(y_N). For a myofibril that consists of N half-sarcomeres, this extension is given by 0.1 $N\Delta t$ μm. We then allow the system to return to mechanical equilibrium, as described earlier. Following this, we proceed from *Determine the number of interacting motors* to *Allow the myofibril to return to mechanical equilibrium*.

Once the stretch is complete, we return to the isometric protocol described in *Isometric activation at half-sarcomere length of 1.5 μm*, and continue until a total time of 5 s had elapsed. Because we assume that heterogeneities in half-sarcomere lengths arise during stretch, $\alpha = 0$ during isometric conditions, and $\alpha = 0.2$ during the stretch.

Stretch of a myofibril, where the stiffness of the nonlinear element increases.

The same protocol as *Isometric activation of a myofibril at an average half-sarcomere of length 1.4 μm, followed by a stretch of 0.1 μm/half-sarcomere* is followed, except that, upon initiation of the stretch, the value of σ in *Eq. 12* is increased by a factor of 1.5.

RESULTS

Intact Fibers

When the intact fibers were activated at L_o, they produced forces of ~140 mN/mm^2 (Figs. 1 and 3), a value that is consistent with previous studies using the diaphragm from mice (16). The fibers underwent several contractions without a loss of contractile capacity. In all bundles investigated in this study, the steady-state forces following active stretch were greater than the isometric force during reference contractions at the corresponding length (L_f) (Fig. 3).

This result was observed for both stretch amplitudes used in this study (4% L_o and 8% L_o). In Fig. 3, it is clear that this RFE is larger when the 8% stretch was applied to the bundles, a result that has been observed previously, i.e., the RFE is dependent on the magnitude of stretch. Note that when the contractions are developed at a longer length, there is a large passive force developed by the fibers, but the RFE is still present (Fig. 3*B*). In all experiments, the steady-state forces following active stretch were always equal or greater than the isometric reference contractions at the length from which the stretch was initiated (L_i) (Fig. 3*C*).

To represent the relationship between force produced by the fibers and the length, we plotted all the experiments after binning the data into sets related to forces produced at the initial length (L_i) and at L_o (Fig. 4, *A* and *B*).

It is clear that a 4% L_o stretch induced a lower RFE than that obtained during an 8% L_o stretch, but while the former tended to remain relatively constant for all the lengths progressively tested; the latter rapidly reached its highest value around the 85% of L_i/P_o, and presented a tendency to decrease quickly, paralleling the 4% values to basically similar values at the last L_i/P_o value investigated (Fig. 4). It is important to note that when the fibers were activated at longer lengths, the force decreased to levels that follow closely the force-length relationship for striated muscles (35), and consistent with other studies that have evaluated this relation for the diaphragm.

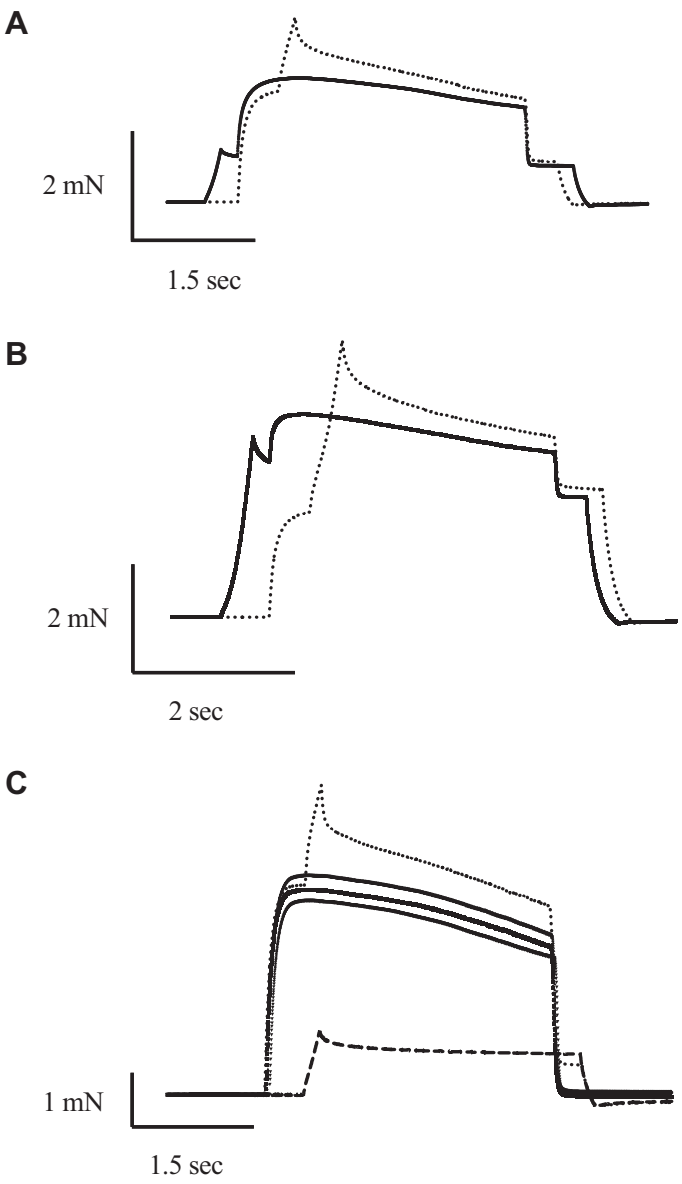

Figure 3. *A* and *B*: typical force traces from the same fiber bundle during passive and active stretches at 4% and 8% L_o stretch amplitude, with stretch durations of 0.2 and 0.4 s, respectively. *C*: contractions reflect the isometric force produced at optimum length (P_o, top isometric trace), the isometric force at the starting length (L_i, middle isometric trace), and the isometric force produced at the final length ($L_{f\text{-}p}$, bottom isometric trace). It also shows the active stretch (L_i +4%, dotted line) and the passive stretch (*p*, bottom trace, traced line).

Figure 4*C* summarizes the levels of RFE observed in all conditions investigated in this study, at different L_i/P_o and with the two amplitudes of stretch (4% and 8%). The RFE was larger with 8% stretches across all lengths, with a significant difference observed at around 85% of L_i/P_o.

Myofibrils

The force produced by myofibrils maximally activated with a pCa^{2+} 4.5, at a sarcomere length 2.7 μm was 136 ± 24 nN/μm^2, in the same range as previous studies with myofibrils isolated from the diaphragm (16) or other

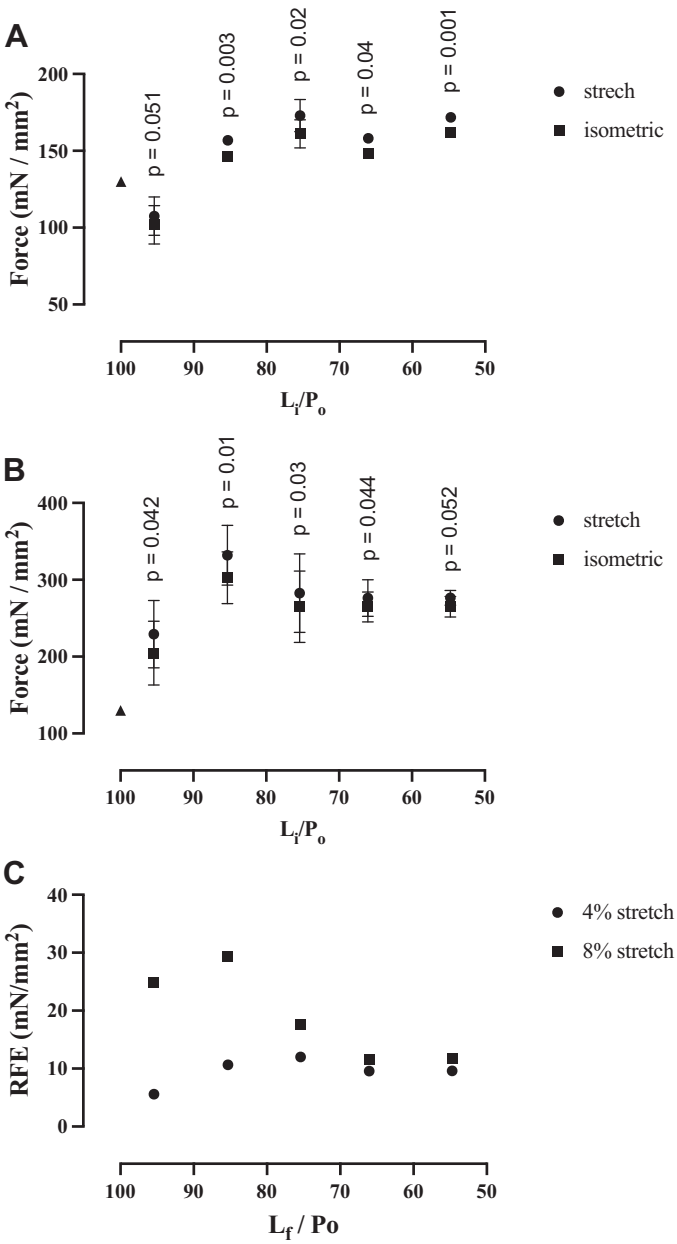

Figure 4. *A* and *B*: the mean values (±SE) for all experiments conducted with the intact fibers, during isometric (squares) and stretch (dots) contractions, in all L_i/P_o ratios investigated. Stretches were performed with an amplitude of 4% (*A*) or 8% (*B*) of L_o. The black triangle indicates the tension at P_0. *C*: the RFE average values of each group are shown. RFE values were obtained subtracting L_i + % from the respective L_f averaged values. Dots and squares represent the values obtained with stretches of 4% and 8% of L_o, respectively, for different L_i/P_o ratios. The *P* values obtained during comparisons performed after ANOVA are shown for each condition. RFE, residual force enhancement.

skeletal muscles (4, 5). When the myofibrils were activated at longer sarcomere lengths (2.8 μm, 2.9 μm, 3.0 μm, and 3.1 μm), the force decreased to levels corresponds to those predicted by the force-sarcomere length relationship (29, 35) (Figs. 5, 6, and 7).

Figure 5 shows force traces recorded during a typical experiment with myofibrils in which they were either activated isometrically or stretched during activation. In this case, myofibrils were stretched from 2.8 μm to 2.9 μm, or from 2.8 μm to 3.0 μm. It is clear that when myofibrils were stretched during activation, RFE was present (Fig. 5, *A* and *B*), a result that was observed consistently across the experiments, and similar to the results observed with intact fibers. The RFE was larger with larger stretches, in agreement with the results obtained with the intact fibers (Fig. 6, *A* and *B* and Fig. 7, *A* and *B*).

Since the force traces are not completely parallel after the stretch, and we cannot activate fibers and myofibrils for very long periods of time without causing damage or fatigue to the preparations, we have performed the following analysis to evaluate when the RFE would cease. We plotted the difference between the stretch forces and the isometric forces from the time the stretch stopped to the time we deactivated the preparations (Fig. 5). We then fitted a third-order polynomial equation to the curve and interpolated to the *x*-axis where force reached zero. In the case of Fig. 5*C*, the force difference drops to zero at 15.3 s after the end of the stretch. Figure 6 shows the average values obtained with these plots for different conditions investigated in this study, and shows that force remains elevated for a long period of time.

Sarcomere Length Dispersion

We measured the dispersion of sarcomere lengths in all myofibrils investigated in this study (Fig. 6, *C* and *D* and Fig. 7, *C* and *D*). The sarcomere length dispersion provides an indication of the nonuniformity of sarcomere lengths induced by activation and stretch of the sarcomeres. The dispersion was small in rested myofibrils, as expected from previous studies. There was an increase in the sarcomere length (SL) dispersion during activation, i.e., during maximal force development in isometric conditions. The increase is consistent with previous studies performed with skeletal muscle myofibrils (5, 29, 36, 37). Most importantly, there was a significant increase in the level of sarcomere length nonuniformity after the stretches were applied to the myofibrils. Similar to what we observed with the force developed by the myofibrils, the increase in sarcomere length dispersion was larger for the stretches performed with larger magnitudes (i.e., equivalent to stretches performed with 8% L_o compared to 4% L_o) (Fig. 8).

Force Enhancement and $Ca^{2\pm}$ Sensitivity

We also tested the myofibrils at 2.9 μm but at different Ca^{2+} concentrations (pCa^{2+}). Figure 9 shows that the force-pCa^{2+} relationship is shifted to the left when stretch contractions are induced to the myofibrils, indicating an increase in the Ca^{2+} sensitivity of the contractile apparatus. The shift was tested statistically by comparisons of the $pCa^{2+}{}_{50}$ in the two curves, i.e., the amount of Ca^{2+} required to produce 50% of maximal force. The shift was significant with $pCa^{2+}{}_{50}$ values of 6.08 ± 0.53 and 5.86 ± 0.25 for the RFE and the isometric contractions, respectively.

Stochastic Model

In Fig. 10, we present the results of our 5-s simulations for a myofibril consisting of 50 half-sarcomeres. When we compare the force produced by a myofibril that is activated isometrically at an average half-sarcomere length of 1.5 μm (Fig. 10 *top*, black line) with a myofibril that is activated

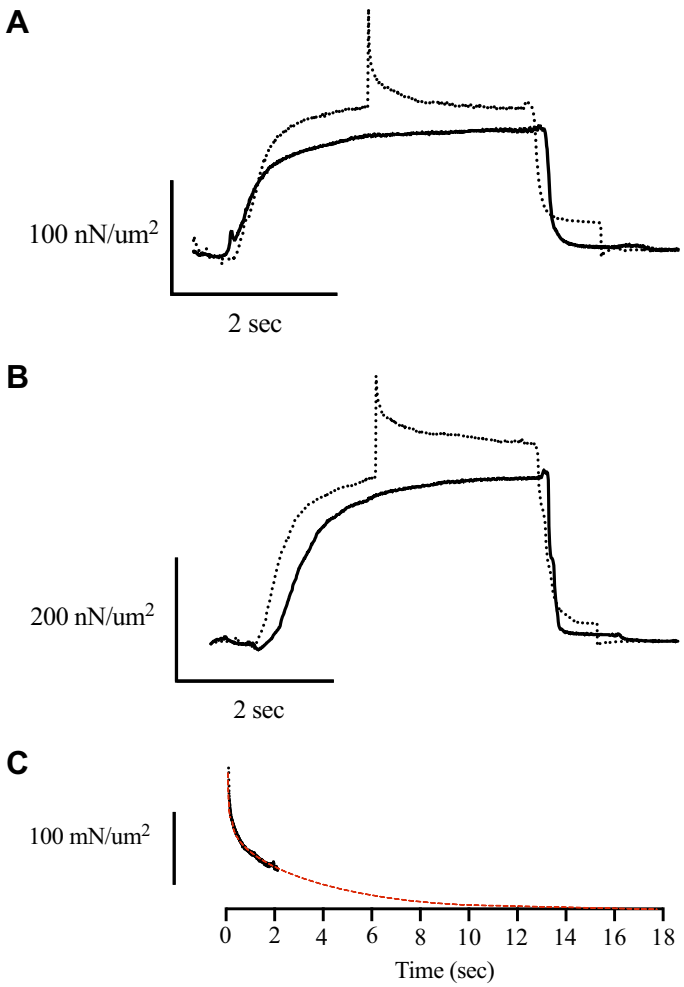

Figure 5. Typical myofibril contractions recorded during an experiment in which they were activated isometrically (solid lines) or stretched during activation (dotted lines). The traces show isometric forces developed at 2.9 μm, and forces developed when myofibrils were stretched from 2.8 μm to 2.9 μm (*A*), and isometric forces developed at 3.0 μm and when myofibrils were stretched from 2.8 μm to 3.0 μm (*B*). It is clear that myofibrils developed RFE in both conditions. *C*: data fitting (red) of the force after the stretch, extrapolated over time to reach force zero. RFE, residual force enhancement.

isometrically at 1.4 μm and then stretched to 1.5 μm (Fig. 10 *top*, red line), we see a significant, persistent RFE. This is associated with an increase in the standard deviation of the half-sarcomere lengths for the stretched fiber (Fig. 9 *bottom*, red line). This effect is enhanced when we increase the stiffness of the nonlinear passive spring upon initiation of the stretch (Fig. 10, blue line).

Taken together, these simulations support the hypothesis that RFE results from both *1*) nonuniformity in half-sarcomere lengths resulting from stretch and *2*) the increase in stiffness of titin that arises when it is stretched following activation.

DISCUSSION

In this study, we investigated the RFE in diaphragm muscle fibers and myofibrils, and its connection to sarcomere-length nonuniformities. We used two complementary techniques that allow the investigation of the RFE in intact fibers and permeabilized myofibrils. Both preparations showed that RFE was present in the diaphragm, and was dependent on the amplitude of the stretch applied to the preparation, such that large stretches led to higher increases in force. RFE showed a different force-length relationship when stretches of different amplitudes were applied to the intact fibers. Furthermore, we observed that RFE was accompanied by *1*) an increase in the degree of sarcomere length nonuniformity and *2*) an increase in the Ca^{2+} sensitivity of the contractile apparatus. We also developed a stochastic, mathematical model and showed that sarcomere nonuniformities induced during a stretch may indeed lead to a residual increase in force, and that can be augmented when we increase the stiffness of titin as a result of myofibril activation and stretch. These results suggest that the RFE is caused by sarcomere length nonuniformities and accompanied by a greater response of the myofibrils to activation, likely due to changes in the properties of titin.

In our experiments, the force developed during an isometric contraction was first allowed to stabilize, upon which stretches of % relative to the starting length of the fibers and myofibril were imposed. The forces obtained after stretch were between 3% and 24% greater than the isometric force developed at the same sarcomere length, similar to previous results (6, 7, 37). Although there are not many studies that carefully compared forces produced by skeletal muscles during contractions while controlling for sarcomere length and sample integrity, those that uses a rigorous experimental protocol report an average RFE of 5%–40% in single fibers (1, 2, 4), myofibrils (6, 7, 37), sarcomeres (30), and half-sarcomeres (7, 8). Our results are particularly revealing because the results from mechanical measures done in intact fibers from the mice, activated through action potentials, were similar to those obtained with individual myofibrils, activated directly with Ca^{2+}.

Interestingly, studies with myofibrils and intact muscles isolated from the heart do not show RFE. They show that stretch increased the force but just after the stretch the force decays to attain a similar level to that observed during regular contractions. The difference in the RFE between skeletal muscles and cardiac muscles has been explained by one of the underlying mechanisms of RFE: an increase in the stiffness of titin upon activation and stretch. The isoforms of titin in skeletal (limb and diaphragm) and cardiac muscles are different. We suggest that activation affects N2A titin isoforms of skeletal myofibrils causing RFE after stretch, but not N2B titin isoforms of cardiac myofibrils, as follows. When the myofibrils are activated, the released Ca^{2+} binds to the I-band region of titin containing proline, glutamate, valine, and lysine (PEVK) that are rich with glutamate domains (E-domains) (12). Consequently, titin reduces its persistence length (38–41), increases its stiffness (12), and produces more force when stretched. The N2A titin isoforms of the skeletal psoas myofibrils have larger PEVK segments with more E-domains than the N2B titin isoforms of the cardiac papillary myofibrils (42, 43). Therefore, skeletal psoas myofibrils are more likely to show an increase of titin force during activation than cardiac myofibrils.

This mechanism aligns with recent studies that show a static tension and directly associate it with residual force

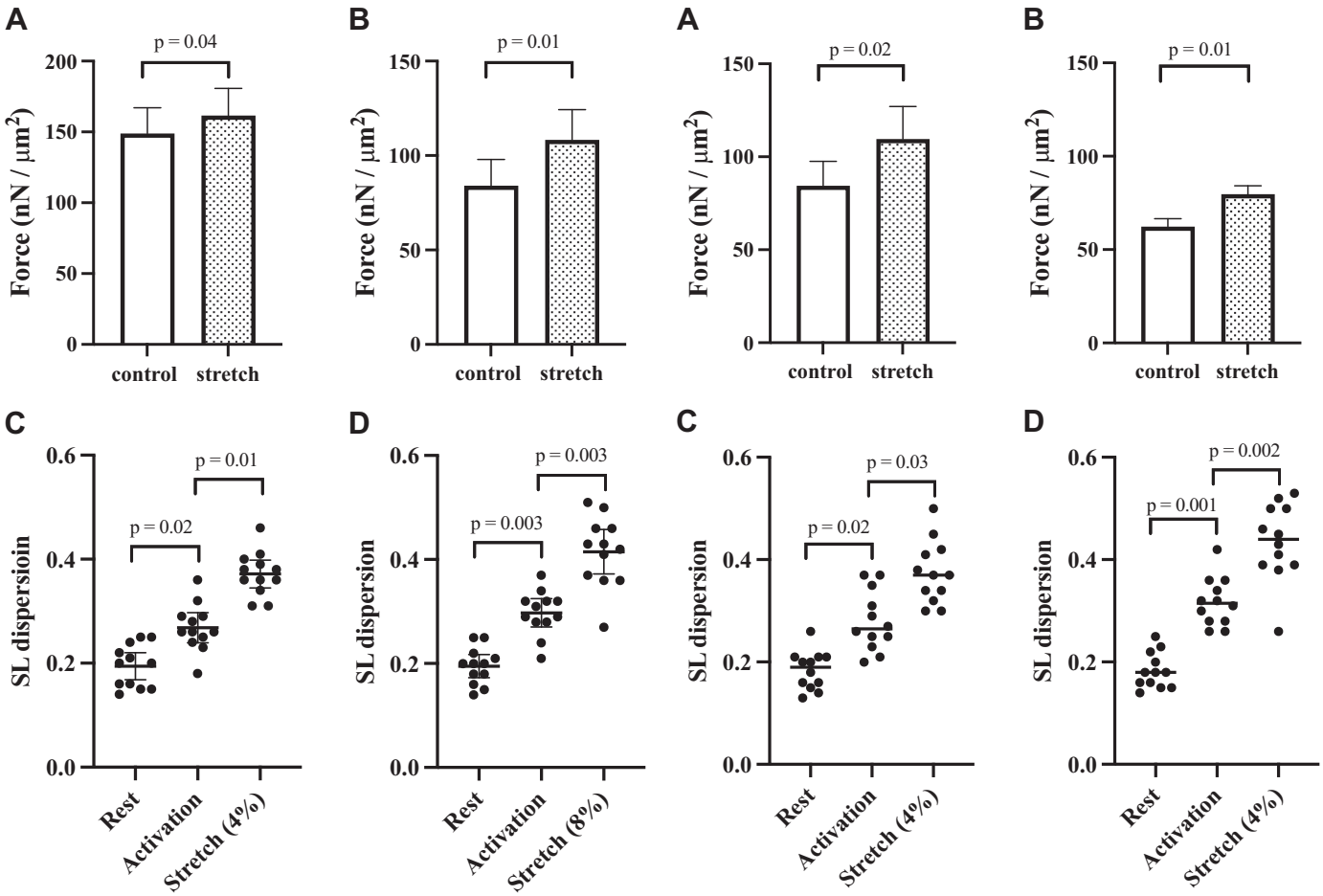

Figure 6. Mean force values of myofibrils produced during isometric contractions developed at 2.8 μm and 2.9 μm (solid lines, *A* and *B*) and after stretch contractions initiated at 2.7 μm (dotted lines, *A* and *B*). The force is significantly higher after stretch in both conditions. The level of sarcomere length nonuniformity during these contractions is represented in *C* and *D*. There is a significant increase in the degree of sarcomere length nonuniformity in myofibrils when they are at rest, during activation, and then after the stretch the results in RFE. The *P* values obtained during comparisons performed after ANOVA are shown for each condition. RFE, residual force enhancement.

Figure 7. Mean force values of myofibrils produced during isometric contractions developed at 2.9 μm and 3.0 μm (solid lines, *A* and *B*) and after stretch contractions initiated at 2.8 μm (dotted lines, *A* and *B*). The force is significantly higher after stretch in both conditions. The level of sarcomere length nonuniformity during these contractions is represented in *C* and *D*. There is a significant increase in the degree of sarcomere length nonuniformity in myofibrils when they are at rest, during activation, and then after the stretch the results in RFE. The *P* values obtained during comparisons performed after ANOVA are shown for each condition.

enhancement in skeletal muscles (4, 18, 44), but not in cardiac muscles (4, 6). The static tension represents an increase in forces that are not derived from cross bridges, but a passive component, likely due to titin—that is evident when skeletal muscles are activated and stretched in the absence of myosin-actin interactions (45). RFE has been a subject of much investigation because it cannot readily be explained within the features of the classic isometric force-sarcomere length relationship (23, 46).

There is also the possibility that Ca^{2+} increases the binding between actin and titin, which would increase the sarcomere stiffness and consequently cause the RFE. It is known that titin binds to actin in PEVK segments and that this binding is regulated by Ca^{2+} (47–51). However, there are studies that show an increase in actin motility over myosin in the presence of titin and Ca^{2+} which suggests that the binding between titin and actin is weakened (49, 52). Another study showed that S100A1, a soluble Ca^{2+}-binding protein highly concentrated in striated muscles hinders actin from interacting with PEVK segments of titin (51), which would prevent an increase of stiffness. Ultimately, the effect of Ca^{2+} on titin binding to actin seems to be inconclusive and requires further investigation.

Intact Fibers and Different Stretch Magnitudes

During all consecutive stretches applied to the intact fibers, RFE was present along the entire force-length relationship (data not shown). Since this study focused on the RFE developed on the descending limb of the force-length relationship, only RFE values starting from L_i corresponding to $\leq$95% P_o were collected for analysis. For all L_i/P_o ratios examined and for both stretch amplitudes tested, RFE was always present but it showed two distinct force-length curves, especially in the first section, after which RFE showed a common trend, to become negligible.

The force-length curves (with 4% or 8% stretches) were different particularly at shorter lengths. The RFE after

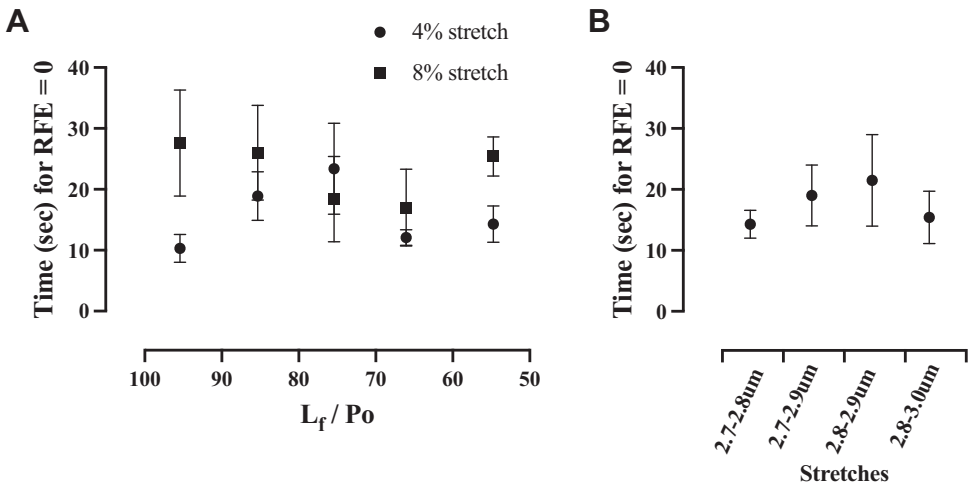

Figure 8. Time in which the RFE dissipates after the stretch in the different conditions investigated in this study, in experiments with fiber bundles (*A*) and myofibrils (*B*). The results were obtained after interpolating the differences between the stretch curves and the isometric curves until force reached zero. They represent the average of all curves plotted for a given situation. The *x*-axes show the different situations investigated during the experiments.

stretches of 4% L_o remained constant for all the L_i/P_o tested, showing that this kind of preparation could well tolerate a certain amount of stretch without losing its capacity to generate active force. In experiments in which we used stretches of 8% L_o, the RFE reached a maximum level in the first part of the descending limb of the force-length relationship, and then it decreases progressively. These results were expected, and consistent with previous findings showing that there is an optimal length for the development of RFE, which is around 2.8 μm–3.0 μm or just beyond the plateau of the force-length relationship (1, 7). In one of these studies, Edman et al. (1) in their study used intact fibers from the frog, a preparation similar to the one we used in this study, and showed results similar to ours—a dependence of the RFE on the stretch magnitude and the initial sarcomere length (their Fig. 5).

Sarcomere Length Nonuniformity

The mechanisms of RFE have been clarified over the past years, and now it is clear that the increase in force is caused partially by sarcomere length nonuniformities that arise upon contraction and stretch of a myofibril (1, 2, 5, 8). When activated, sarcomeres at different lengths elicit different responses—shorter, stronger sarcomeres will contract more quickly, at the expense of longer, weaker sarcomeres that will stretch (2, 53). Imposing a stretch during an active contraction exaggerates these irregularities in sarcomere lengths; strong sarcomeres will have a favorable overlap, producing higher active forces, whereas weak sarcomeres elongate to greater lengths shifting their contribution to the overall force output increasingly towards large passive forces. This scenario allows for an increase in the total force: shorter sarcomeres have a larger number of myosin heads attached to actin, producing more active force. The sarcomeres that will be stretched lose filament overlap but will have a greater stiffness due to the elongation of titin, which acts as a spring-like molecule and is responsible for passive forces in sarcomeres. The overall force produced by both the shorter sarcomeres with more cross-bridge interaction and the longer sarcomeres with a large passive force will be higher than the force produced during isometric contractions.

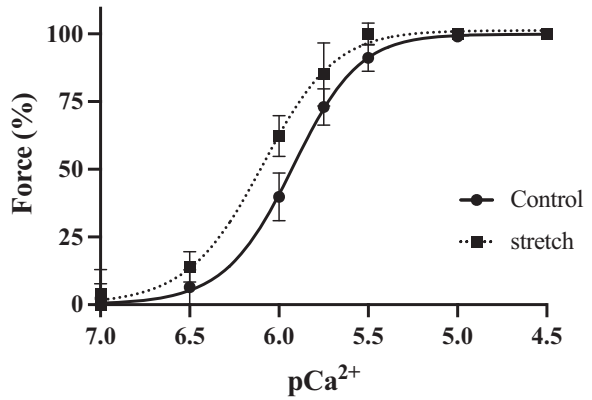

Figure 9. The force-pCa^{2+} relationship derived from force values developed during isometric contractions (solid line) and after stretches (dotted line). All values were recorded at a final sarcomere length of 2.9 μm. There is shift in the curve to the left, indicating that the Ca^{2+} sensitivity of the contractile apparatus is increased in conditions of RFE. The $pCa^{2+}{}_{50}$ was significantly different between the wo conditions ($P = 0.01$). RFE, residual force enhancement.

We observed that the RFE was accompanied by an increase in sarcomere length nonuniformity, a result that has been observed previously in myofibrils from the psoas muscle (5). In that study, we induced nonuniformity in myofibrils by depleting the thick filament from a target sarcomere, which increased significantly the sarcomere length nonuniformity. The result was a decline in isometric force with the inactivation of contractile proteins in one sarcomere, and an increase in nonuniformity. Most importantly, the RFE was ~20% higher in these myofibrils compared with the isometric force produced at the same sarcomere length. Although control myofibrils produce a residual force enhancement of ~5%, myofibrils with one inactive sarcomere show four times larger levels of residual force enhancement (5).

Some myofibrils in the current study showed a negligible amount of sarcomere length nonuniformity, and yet still produced a small degree of RFE. These results suggest that nonuniformity is, in part, connected to residual force enhancement, but that it cannot account for the phenomenon in its entirety. Furthermore, the occurrence of RFE in single sarcomeres and half-sarcomeres—preparations in

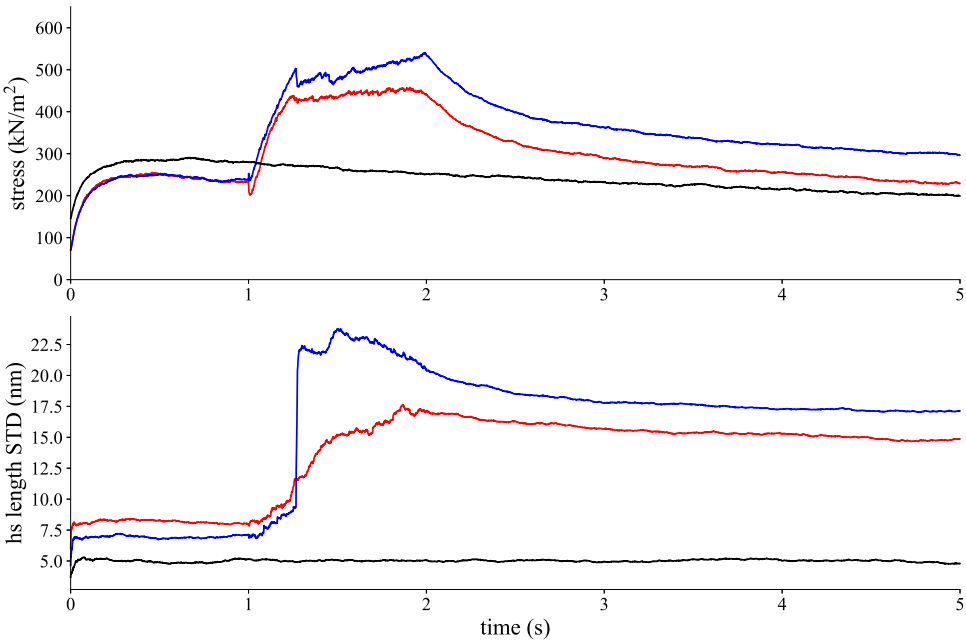

Figure 10. Time traces of the stress (*top*) and standard deviation of half-sarcomere length (*bottom*) for a myofibril consisting of 50 half-sarcomeres. The black curve is for a myofibril that is activated under isometric conditions, with an average half-sarcomere length of 1.5 μm. The red curve describes a myofibril that is first activated under isometric conditions, with an average half-sarcomere length of 1.4 μm, and then stretched starting at $t = 1$ s at a rate of 0.1 μm/s/half-sarcomere until it reaches an average half-sarcomere length of 1.5 μm. The blue curve describes a myofibril that undergoes the same stretching process as described by the red curve, except that the stiffness of the nonlinear passive spring is increased upon initiation of the stretch.

which nonuniformity is naturally absent—also suggests an alternate mechanism for enhanced forces after stretch (7, 8).

A possible explanation is centered around the Ca^{2+}-dependent increase in stiffness of the elastic protein titin. When Ca^{2+} levels rise during activation of myofibrils, Ca^{2+} binds to the PEVK-domains of titin, which consequently reduces its persistence length (12). This leads to an increase in the stiffness of titin and a subsequently higher contribution of passive forces to the total force output after an imposed stretch. When a myofibril is stretched, the stiffness of titin will increase further causing a larger level of passive force contribution to the total force. This mechanism has been investigated in recent studies that linked levels of a static tension, that cannot be accounted for myosin-actin interactions, to the amount of residual force enhancement seen in myofibrils and muscle fibers (4, 13, 45). Interestingly, myofibrils isolated from muscles containing different titin isoforms present different responses to stretch. Studies specifically designed to compare different muscle types showed that myofibrils isolated from the soleus and psoas show residual force enhancement that is accompanied by an increase in the static stiffness, whereas cardiac myofibrils do not show residual force enhancement (4, 6). The difference may be related to the physiological role. Cardiac muscles are not stretched while contracting in vivo, and thus a residual force enhancement caused by a Ca^{2+}-dependent increase in titin stiffness would not play a physiological role during contractions. This interpretation is strengthened by a recent study showing that intact cardiac trabeculae also do not present a residual force enhancement after stretch (9).

Tellingly, our stochastic model showed that force enhancement can be produced by myofibrils when *1*) we induce sarcomere length nonuniformities and *2*) we increase the static stiffness, or the stiffness produced by titin during activation and stretch. In the latter case, we observed larger levels of RFE, strengthening our hypotheses.

$Ca^{2\pm}$ Sensitivity of the Contractile Apparatus

The Ca^{2+} sensitivity was increased in myofibrils during the RFE, showing that the stretch leads to a greater force produced for a given level of Ca^{2+} activation. The increased Ca^{2+} sensitivity is on line with two mechanisms already discussed in this paper: an increase in sarcomere length nonuniformity and an increase in the titin-based increase in stiffness—which have been recognized as the two mechanisms of RFE (54, 55). First, there is a length-dependence of the force-pCa^{2+} relationship (56–58), such that submaximal contractions increase their force when activated at long sarcomere lengths, even with a decrease in filament overlap. Thus, an increase in individual sarcomere lengths caused by sarcomere length nonuniformity would increase the Ca^{2+} sensitivity of the myofibrils. Second, the titin-induced passive force is an important contributor to the increase in Ca^{2+} sensitivity at long sarcomere lengths (59–61). Although there are no other studies investigating the Ca^{2+} sensitivity of the contractile apparatus in myofibrils, it has been shown that the level of muscle activation influences directly the RFE; stretches invoked in low Ca^{2+} concentrations lead to a larger RFE than large Ca^{2+} concentrations (3).

ACKNOWLEDGMENTS

The authors thank Dr. Claudio Pregno for the precious technical support with the experiments with the intact muscle fibers. D.E. Rassier is a Canada Research Chair in Muscle Biophysics.

GRANTS

This study was supported by National Sciences and Engineering Research Council (NSERC) Canada and by University of Florence (ex 60%-Bagni, Contini 2021), Italy.

DISCLOSURES

No conflicts of interest, financial or otherwise, are declared by the authors.

AUTHOR CONTRIBUTIONS

M.C., D.A., D.E.R., and M.A.B. conceived and designed research; M.C., A.C., and M.A.B. performed experiments; M.C., D.A., A.C., and M.A.B. analyzed data; M.C., D.A., A.C., D.E.R., and M.A.B. interpreted results of experiments; M.C., D.A., D.E.R., and M.A.B. prepared figures; M.C., D.E.R., and M.A.B. drafted manuscript; M.C., D.A., A.C., D.E.R., and M.A.B. edited and revised manuscript; M.C., D.A., A.C., D.E.R., and M.A.B. approved final version of manuscript.

REFERENCES

1. **Edman KA**, **Elzinga G**, **Noble MI.** Residual force enhancement after stretch of contracting frog single muscle fibers. *J Gen Physiol* 80: 769–784, 1982. doi:10.1085/jgp.80.5.769.
2. **Julian FJ**, **Morgan DL.** The effect on tension of non-uniform distribution of length changes applied to frog muscle fibres. *J Physiol* 293: 379–392, 1979. doi:10.1113/jphysiol.1979.sp012895.
3. **Minozzo FC**, **Rassier DE.** The effects of Ca2 + and MgADP on force development during and after muscle length changes. *PloS one* 8: e68866, 2013. doi:10.1371/journal.pone.0068866.
4. **Cornachione AS**, **Leite F**, **Bagni MA**, **Rassier DE.** The increase in non-cross-bridge forces after stretch of activated striated muscle is related to titin isoforms. *Am J Physiol Cell Physiol* 310: C19–26, 2016. doi:10.1152/ajpcell.00156.2015.
5. **Haeger RM**, **Rassier DE.** Force enhancement after stretch of isolated myofibrils is increased by sarcomere length non-uniformities. *Sci Rep* 10: 21590, 2020. doi:10.1038/s41598-020-78457-1.
6. **Shalabi N**, **Cornachione A**, **de Souza Leite F**, **Vengallatore S**, **Rassier DE.** Residual force enhancement is regulated by titin in skeletal and cardiac myofibrils. *J Physiol* 595: 2085–2098, 2017. doi:10.1113/JP272983.
7. **Rassier DE**, **Pavlov I.** Force produced by isolated sarcomeres and half-sarcomeres after an imposed stretch. *Am J Physiol Cell Physiol* 302: C240–C248, 2012 [Erratum in *Am J Physiol Cell Physiol*. 302: C835–C836, 2012]. doi:10.1152/ajpcell.00208.2011.
8. **Minozzo FC**, **Baroni BM**, **Correa JA**, **Vaz MA**, **Rassier DE.** Force produced after stretch in sarcomeres and half-sarcomeres isolated from skeletal muscles. *Sci Rep* 3: 2320, 2013. doi:10.1038/srep02320.
9. **Tomalka A**, **Rohrle O**, **Han JC**, **Pham T**, **Taberner AJ**, **Siebert T.** Extensive eccentric contractions in intact cardiac trabeculae: revealing compelling differences in contractile behaviour compared to skeletal muscles. *Proc Biol Sci* 286: 20190719, 2019. doi:10.1098/rspb.2019.0719.
10. **Edman KA.** Residual force enhancement after stretch in striated muscle. A consequence of increased myofilament overlap? *J Physiol* 590: 1339–1345, 2012. doi:10.1113/jphysiol.2011.222729.
11. **de Souza Leite F**, **Rassier DE.** Sarcomere length nonuniformity and force regulation in myofibrils and sarcomeres. *Biophys J* 119: 2372–2377, 2020. doi:10.1016/j.bpj.2020.11.005.
12. **Labeit D**, **Watanabe K**, **Witt C**, **Fujita H**, **Wu Y**, **Lahmers S**, **Funck T**, **Labeit S**, **Granzier H.** Calcium-dependent molecular spring elements in the giant protein titin. *Proc Natl Acad Sci USA* 100: 13716–13721, 2003. doi:10.1073/pnas.2235652100.
13. **Cornachione AS**, **Rassier DE.** A non-cross-bridge, static tension is present in permeabilized skeletal muscle fibers after active force inhibition or actin extraction. *Am J Physiol Cell Physiol* 302: C566–C574, 2012. doi:10.1152/ajpcell.00355.2011.
14. **Coirault C**, **Chemla D**, **Pourny JC**, **Lambert F**, **Lecarpentier Y.** Instantaneous force-velocity-length relationship in diaphragmatic sarcomere. *J Appl Physiol (1985)* 82: 404–412, 1997. doi:10.1152/jappl.1997.82.2.404.
15. **Allen DG**, **Lannergren J**, **Westerblad H.** Intracellular ATP measured with luciferin/luciferase in isolated single mouse skeletal muscle fibres. *Pflugers Arch* 443: 836–842, 2002. doi:10.1007/s00424-001-0756-y.
16. **Bagni MA**, **Colombini B**, **Nocella M**, **Pregno C**, **Cornachione AS**, **Rassier DE.** The effects of fatigue and oxidation on contractile function of intact muscle fibers and myofibrils isolated from the mouse diaphragm. *Sci Rep* 9: 4422, 2019. doi:10.1038/s41598-019-39353-5.
17. **Colombini B**, **Benelli G**, **Nocella M**, **Musaro A**, **Cecchi G**, **Bagni MA.** Mechanical properties of intact single fibres from wild-type and MLC/mIgf-1 transgenic mouse muscle. *J Muscle ResCell Motil* 30: 199–207, 2009. doi:10.1007/s10974-009-9187-8.
18. **Nocella M**, **Cecchi G**, **Bagni MA**, **Colombini B.** Force enhancement after stretch in mammalian muscle fiber: no evidence of cross-bridge involvement. *Am J Physiol Cell Physiol* 307: C1123–C1129, 2014. doi:10.1152/ajpcell.00290.2014.
19. **Rassier DE**, **Minozzo FC.** Length-dependent Ca2 + activation in skeletal muscle fibers from mammalians. *Am J Physiol Cell Physiol* 311: C201–C211, 2016. doi:10.1152/ajpcell.00046.2016.
20. **Persson M**, **Steinz MM**, **Westerblad H**, **Lanner JT**, **Rassier DE.** Force generated by myosin cross-bridges is reduced in myofibrils exposed to ROS/RNS. *Am J Physiol Cell Physiol* 317: C1304–C1312, 2019. doi:10.1152/ajpcell.00272.2019.
21. **Shalabi N**, **Persson M**, **Mansson A**, **Vengallatore S**, **Rassier DE.** Sarcomere stiffness during stretching and shortening of rigor skeletal myofibrils. *Biophys J* 113: 2768–2776, 2017. doi:10.1016/j.bpj.2017.10.007.
22. **Allen DG**, **Westerblad H.** The effects of caffeine on intracellular calcium, force and the rate of relaxation of mouse skeletal muscle. *J Physiol* 487: 331–342, 1995. doi:10.1113/jphysiol.1995.sp020883.
23. **Bagni MA**, **Cecchi G**, **Colomo F**, **Tesi C.** Plateau and descending limb of the sarcomere length-tension relation in short length-clamped segments of frog muscle fibres. *J Physiol* 401: 581–595, 1988. doi:10.1113/jphysiol.1988.sp017181.
24. **Nocella M**, **Colombini B**, **Benelli G**, **Cecchi G**, **Bagni MA**, **Bruton J.** Force decline during fatigue is due to both a decrease in the force per individual cross-bridge and the number of cross-bridges. *J Physiol* 589: 3371–3381, 2011. doi:10.1113/jphysiol.2011.209874.
25. **Rassier DE.** Pre-power stroke cross bridges contribute to force during stretch of skeletal muscle myofibrils. *Proc Biol Sci* 275: 2577–2586, 2008. doi:10.1098/rspb.2008.0719.
26. **Ribeiro PA**, **Ribeiro JP**, **Minozzo FC**, **Pavlov I**, **Leu NA**, **Kurosaka S**, **Kashina A**, **Rassier DE.** Contractility of myofibrils from the heart and diaphragm muscles measured with atomic force cantilevers: effects of heart-specific deletion of arginyl-tRNA-protein transferase. *Int J Cardiol* 168: 3564–3571, 2013. doi:10.1016/j.ijcard.2013.05.069.
27. **Labuda A**, **Brastaviceanu T**, **Pavlov I**, **Paul W**, **Rassier DE.** Optical detection system for probing cantilever deflections parallel to a sample surface. *Rev Sci Instrum* 82: 013701, 2011. doi:10.1063/1.3527913.
28. **Yamada T**, **Fedotovskaya O**, **Cheng AJ**, **Cornachione AS**, **Minozzo FC**, **Aulin C**, **Friden C**, **Turesson C**, **Andersson DC**, **Glenmark B**, **Lundberg IE**, **Rassier DE**, **Westerblad H**, **Lanner JT.** Nitrosative modifications of the Ca2 + release complex and actin underlie arthritis-induced muscle weakness. *Ann Rheum Dis* 74: 1907–1914, 2015. doi:10.1136/annrheumdis-2013-205007.
29. **de Souza Leite F**, **Minozzo FC**, **Altman D**, **Rassier DE.** Microfluidic perfusion shows intersarcomere dynamics within single skeletal muscle myofibrils. *Proc Natl Acad Sci USA* 114: 8794–8799, 2017. doi:10.1073/pnas.1700615114.
30. **Campbell KS.** Interactions between connected half-sarcomeres produce emergent mechanical behavior in a mathematical model of muscle. *PLoS Comput Biol* 5: e1000560, 2009. doi:10.1371/journal.pcbi.1000560.
31. **Bell GI.** Models for the specific adhesion of cells to cells. *Science* 200: 618–627, 1978. doi:10.1126/science.347575.
32. **Guo B**, **Guilford WH.** Mechanics of actomyosin bonds in different nucleotide states are tuned to muscle contraction. *Proc Natl Acad Sci USA* 103: 9844–9849, 2006. doi:10.1073/pnas.0601255103.
33. **Linari M**, **Caremani M**, **Piperio C**, **Brandt P**, **Lombardi V.** Stiffness and fraction of Myosin motors responsible for active force in permeabilized muscle fibers from rabbit psoas. *Biophys J* 92: 2476–2490, 2007. doi:10.1529/biophysj.106.099549.
34. **Virtanen P**, **Gommers R**, **Oliphant TE**, **Haberland M**, **Reddy T**, **Cournapeau D**, **SciPy 1.0 Contributors**, et al. SciPy 1.0: fundamental algorithms for scientific computing in Python. *Nat Methods* 17: 261–272, 2020 [Erratum in *Nat Methods* 17: 352, 2020]. doi:10.1038/s41592-019-0686-2.
35. **Pavlov I**, **Novinger R**, **Rassier DE.** The mechanical behavior of individual sarcomeres of myofibrils isolated from rabbit psoas muscle. *Am J Physiol Cell Physiol* 297: C1211–C1219, 2009. doi:10.1152/ajpcell.00233.2009.
36. **Haeger R**, **de Souza Leite F**, **Rassier DE.** Sarcomere length non-uniformities dictate force production along the descending limb of the

force-length relation. *Proc Biol Sci* 287: 20202133, 2020. doi:10.1098/rspb.2020.2133.
37. **Pun C**, **Syed A**, **Rassier DE.** History-dependent properties of skeletal muscle myofibrils contracting along the ascending limb of the force-length relationship. *Proc Biol Sci* 277: 475–484, 2010. doi:10.1098/rspb.2009.1579.
38. **Kolmerer B**, **Olivieri N**, **Witt CC**, **Herrmann BG**, **Labeit S.** Genomic organization of M line titin and its tissue-specific expression in two distinct isoforms. *J Mol Biol* 256: 556–563, 1996. doi:10.1006/jmbi.1996.0108.
39. **Takahashi K**, **Hattori A**, **Tatsumi R**, **Takai K.** Calcium-induced splitting of connectin filaments into beta-connectin and a 1,200-kDa subfragment. *J Biochem* 111: 778–782, 1992. doi:10.1093/oxfordjournals.jbchem.a123835.
40. **Tatsumi R**, **Hattori A**, **Takahashi K.** Splitting of connectin/titin filaments into beta-connectin/T2 and a 1,200-kDa subfragment by 0.1 mM calcium ions. *Ad Biophys* 33: 65–77, 1996. doi:10.1016/S0065-227X(96)90023-4.
41. **Tatsumi R**, **Maeda K**, **Hattori A**, **Takahashi K.** Calcium binding to an elastic portion of connectin/titin filaments. *J Muscle Res Cell Motil* 22: 149–162, 2001. doi:10.1023/A:1010349416723.
42. **Bang ML**, **Centner T**, **Fornoff F**, **Geach AJ**, **Gotthardt M**, **McNabb M**, **Witt CC**, **Labeit D**, **Gregorio CC**, **Granzier H**, **Labeit S.** The complete gene sequence of titin, expression of an unusual approximately 700-kDa titin isoform, and its interaction with obscurin identify a novel Z-line to I-band linking system. *Circ Res* 89: 1065–1072, 2001. doi:10.1161/hh2301.100981.
43. **Labeit S**, **Kolmerer B.** Titins: giant proteins in charge of muscle ultrastructure and elasticity. *Science* 270: 293–296, 1995. doi:10.1126/science.270.5234.293.
44. **Rassier DE**, **Leite FS**, **Nocella M**, **Cornachione AS**, **Colombini B**, **Bagni MA.** Non-crossbridge forces in activated striated muscles: a titin dependent mechanism of regulation? *J Muscle Res Cell Motil* 36: 37–45, 2015. doi:10.1007/s10974-014-9397-6.
45. **Nocella M**, **Colombini B**, **Bagni MA**, **Bruton J**, **Cecchi G.** Non-cross-bridge calcium-dependent stiffness in slow and fast skeletal fibres from mouse muscle. *J Muscle Res Cell Motil* 32: 403–409, 2012. doi:10.1007/s10974-011-9274-5.
46. **Gordon AM**, **Huxley AF**, **Julian FJ.** The variation in isometric tension with sarcomere length in vertebrate muscle fibres. *J Physiol* 184: 170–192, 1966. doi:10.1113/jphysiol.1966.sp007909.
47. **Kellermayer MS**, **Granzier HL.** Calcium-dependent inhibition of in vitro thin-filament motility by native titin. *FEBS Lett* 380: 281–286, 1996. doi:10.1016/0014-5793(96)00055-5.
48. **Kellermayer MS**, **Granzier HL.** Elastic properties of single titin molecules made visible through fluorescent F-actin binding. *Biochem Biophys Res Commun* 221: 491–497, 1996. doi:10.1006/bbrc.1996.0624.
49. **Kulke M**, **Fujita-Becker S**, **Rostkova E**, **Neagoe C**, **Labeit D**, **Manstein DJ**, **Gautel M**, **Linke WA.** Interaction between PEVK-titin and actin filaments: origin of a viscous force component in cardiac myofibrils. *Circ Res* 89: 874–881, 2001. doi:10.1161/hh2201.099453.
50. **Linke WA**, **Kulke M**, **Li H**, **Fujita-Becker S**, **Neagoe C**, **Manstein DJ**, **Gautel M**, **Fernandez JM.** PEVK domain of titin: an entropic spring with actin-binding properties. *J Struct Biol* 137: 194–205, 2002. doi:10.1006/jsbi.2002.4468.
51. **Yamasaki R**, **Berri M**, **Wu Y**, **Trombitas K**, **McNabb M**, **Kellermayer MS**, **Witt C**, **Labeit D**, **Labeit S**, **Greaser M**, **Granzier H.** Titin-actin interaction in mouse myocardium: passive tension modulation and its regulation by calcium/S100A1. *BiophysJ* 81: 2297–2313, 2001. doi:10.1016/S0006-3495(01)75876-6.
52. **Stuyvers BD**, **Miura M**, **Jin JP**, **ter Keurs HE.** Ca(2+)-dependence of diastolic properties of cardiac sarcomeres: involvement of titin. *Progr Biophys Mol Biol* 69: 425–443, 1998. doi:10.1016/s0079-6107(98)00018-2.
53. **Edman KA**, **Reggiani C.** Redistribution of sarcomere length during isometric contraction of frog muscle fibres and its relation to tension creep. *J Physiol* 351: 169–198, 1984. doi:10.1113/jphysiol.1984.sp015240.
54. **Rassier DE.** The mechanisms of the residual force enhancement after stretch of skeletal muscle: non-uniformity in half-sarcomeres and stiffness of titin. *Proc Biol Sci* 279: 2705–2713, 2012. doi:10.1098/rspb.2012.0467.
55. **Rassier DE.** Residual force enhancement in skeletal muscles: one sarcomere after the other. *J Muscle Res Cell Motil* 33: 155–165, 2012. doi:10.1007/s10974-012-9308-7.
56. **Martyn DA**, **Coby R**, **Huntsman LL**, **Gordon AM.** Force-calcium relations in skinned twitch and slow-tonic frog muscle fibres have similar sarcomere length dependencies. *J Muscle Res Cell Motil* 14: 65–75, 1993. doi:10.1007/BF00132181.
57. **Martyn DA**, **Gordon AM.** Length and myofilament spacing-dependent changes in calcium sensitivity of skeletal fibres: effects of pH and ionic strength. *J Muscle Res Cell Motil* 9: 428–445, 1988. doi:10.1007/BF01774069.
58. **McDonald KS**, **Moss RL.** Osmotic compression of single cardiac myocytes eliminates the reduction in Ca2+ sensitivity of tension at short sarcomere length. *Circ Res* 77: 199–205, 1995. doi:10.1161/01.RES.77.1.199.
59. **Cazorla O**, **Wu Y**, **Irving TC**, **Granzier H.** Titin-based modulation of calcium sensitivity of active tension in mouse skinned cardiac myocytes. *Circ Res* 88: 1028–1035, 2001. doi:10.1161/hh1001.090876.
60. **Terui T**, **Sodnomtseren M**, **Matsuba D**, **Udaka J**, **Ishiwata S**, **Ohtsuki I**, **Kurihara S**, **Fukuda N.** Troponin and titin coordinately regulate length-dependent activation in skinned porcine ventricular muscle. *J Gen Physiol* 131: 275–283, 2008. doi:10.1085/jgp.200709895.
61. **Udaka J**, **Ohmori S**, **Terui T**, **Ohtsuki I**, **Ishiwata S**, **Kurihara S**, **Fukuda N.** Disuse-induced preferential loss of the giant protein titin depresses muscle performance via abnormal sarcomeric organization. *J Gen Physiol* 131: 33–41, 2008. doi:10.1085/jgp.200709888.